Compositions of Gamma and Gamma Prime Phases in an As-Cast Nickel-Based Single Crystal Superalloy Turbine Blade

Park, Keehyun; Withey, Paul

DOI:
10.3390/cryst12020299

Document Version
Publisher's PDF, also known as Version of record

Citation for published version (Harvard):
Park, K & Withey, P 2022, 'Compositions of Gamma and Gamma Prime Phases in an As-Cast Nickel-Based Single Crystal Superalloy Turbine Blade', *Crystals*, vol. 12, no. 2, 299. https://doi.org/10.3390/cryst12020299

crystals

MDPI

Article

Compositions of Gamma and Gamma Prime Phases in an As-Cast Nickel-Based Single Crystal Superalloy Turbine Blade

KeeHyun Park * and Paul Withey

School of Metallurgy and Materials, University of Birmingham, Birmingham B15 2TT, UK; p.a.withey@bham.ac.uk
* Correspondence: k.park.2@bham.ac.uk

Abstract: The core and the interdendritic regions of an as-cast nickel based single crystal turbine blade were observed by electron microscopy to understand the microstructural development during an investment casting process. The dendrite core region shows an irregular morphology of gamma prime in gamma due to a relatively short casting time, which prevented the development of gamma prime expected in a solution heat-treated microstructure. By comparison, the interdendritic region comprises three different regions composed of: several elongated gamma prime particles, relatively tiny and irregular gamma prime, and gamma prime with relatively regular morphology. The chemical analysis of these phases showed that, regardless of the analysis point in the core or the interdendritic region, almost the same compositions were acquired in the regular type of gamma and gamma prime phases. This result suggests that if the gamma prime forms in the gamma matrix, the composition of gamma prime is almost uniform regardless of the region and prevailing general chemical composition. In contrast, the composition of the elongated gamma prime in the interdendritic region was slightly different depending on the analysis point even within the same elongated particle.

Keywords: superalloys; microstructure; dendrite core; interdendritic region; chemical composition

Citation: Park, K.; Withey, P. Compositions of Gamma and Gamma Prime Phases in an As-Cast Nickel-Based Single Crystal Superalloy Turbine Blade. *Crystals* **2022**, *12*, 299. https://doi.org/10.3390/cryst12020299

Academic Editor: Cyril Cayron

Received: 7 February 2022
Accepted: 16 February 2022
Published: 20 February 2022

1. Introduction

Ni-based single crystal superalloys have been designed to maximise the combination of significantly high mechanical strength and surface stability at high operating temperatures, allowing severe mechanical stressing to nearly 80% of the melting point, and are thus ideal for turbine blade applications [1–4]. The superior properties of the superalloy are mainly due to two hardening mechanisms: one is solid-solution hardening by the addition of different soluble elements, such as cobalt, chromium, molybdenum, tungsten and rhenium, and the other is precipitation hardening by the relatively uniform precipitation of high volume fractions of the ordered γ' phase (Ni_3(Al, Ta, Ti)) in the face-centred cubic structure matrix (γ phase) [1,3–9]. To maximise design flexibility and minimise manufacturing cost, current Ni-based superalloy turbine blades are produced by investment casting, which can produce hollow aerofoils with complex internal cooling passages, and for the highest performance, eliminate grain boundaries [4]. The casting process forms dendrites, containing the primary phase of γ and fine γ' precipitates, with a specific direction of {001}, followed by eutectic γ and γ' in the interdendritic region. This mixed microstructure is undesirable in the highest performing turbine components, due to an inhomogeneous chemical distribution, which consequently requires homogenisation during the subsequent heat treatment [10]. Therefore, a number of studies have investigated the interdendritic γ and γ', and the casting microsegregation, in order to tune the homogenisation cycle to remove them [11,12].

EPMA (electron probe micro-analysis) using X-ray wavelength dispersive spectroscopy (WDS) has been widely used to analyse the chemical composition of the interdendritic γ and γ' due to the size of the dendritic microstructure in an as-cast turbine blade. For

accurate analysis, multiple WDX points scans were performed, and the compositions of γ and γ' in dendrite core and interdendritic regions, and the partitioning behaviour of alloying elements, were then averaged [11,12]. During EPMA analysis, a focused electron beam (typical energy = 5–30 keV) bombards a micro-volume of a targeted sample, and X-ray photons emitted near the surface are then collected and identified by WDS spectra [13]. Generally, the spot size of the electron beam is 10 µm at an accelerating voltage of 20 kV and a beam current of 100 nA [11] or, in an extreme analysis case, the beam diameter is approximately 1 to 2 µm [14]. In addition, when the electron beam bombards the target, there is an interaction volume of beam/sample with a depth range of a few micrometres depending on the acceleration voltage of the electron beam and the atomic number of the targeted sample [15,16]. However, in nickel-based single crystal superalloy turbine blades, the size of the γ phase, formed as γ channels, is just a few hundreds of nanometres, which means that the spot size of the electron beam and the interaction volume of beam/sample are much larger than that of the γ phase. As a result, even though the electron beam is targeted to bombard just the thin γ phase, it is inevitable that the analysis includes a number of X-ray photons emitted from the surrounding bulky γ' in the chemical composition analysis using EPMA.

Another analysis technique for the compositions of γ and γ' is the use of TEM due to their fine sizes. As it is hard to access the correct location, i.e., the dendrite core or the interdendritic region, with conventional TEM sample preparation techniques, a focused ion beam (FIB) lift-out technique has been widely used to fabricate TEM samples [17–22]. Even though a lamella can be fabricated precisely from the core or the interdendritic region, its size is usually just about 10 µm, which means that one lamella cannot completely contain the two regions. Therefore, two different lamellae need to be fabricated—one from the core, the other from the interdendritic region—in order to investigate the microstructure and the compositions of γ and γ' in the core and the interdendritic region. However, there is the possibility of the contamination of the first lamella during the fabrication of the second sample, even though this contamination may be minor, which may affect the compositional analysis. In addition, it is hard to make two lamellae with almost the same thickness. Importantly, during TEM observation, it is almost impossible to observe two lamellae under the same observation and analysis conditions. Therefore, in this study, a modified TEM sampling method using a FIB lift-out technique was used to make two lamellae on one TEM grid, and the microstructure and the compositions of γ and γ' in the core and the interdendritic region were investigated by electron microscopy.

2. Experiment

Nickel-based single crystal turbine blades were commercially manufactured in an aerospace production manufacturing facility at Rolls-Royce plc. In this study, a third-generation superalloy (CMSX-10N, Cannon Muskegon Corp., Muskegon, MI, USA) was used and the composition is summarised in Table 1. The detailed casting condition and procedure have been described elsewhere in detail [1,11,12].

Table 1. Compositions (at. pct.) of raw material, γ and γ' phases measured in as-cast or fully heat-treated blades [19,20] by STEM-EDX.

Element	Raw	As-Cast Core		As-Cast Interdendritic			Fully Heat-Treated	
		γ	γ'	γ	γ'	Elongated γ'	γ	γ'
Al	13.6	7.4	15.1	6.9	15.3	17.8 ± 2.1	6.3	15.6
Ti	0.1	0.1	0.1	0.1	0.2	0.2 ± 0.1	0.0	0.1
Cr	1.8	4.4	1.1	4.8	1.1	1.1 ± 0.2	4.1	1.0
Co	3.2	5.1	2.4	5.3	2.7	2.4 ± 0.2	5.9	2.7
Nb	0.0 *	0.1	0	0.1	0	0.1	0.0	0.0

Table 1. *Cont.*

Element	Raw	As-Cast Core		As-Cast Interdendritic			Fully Heat-Treated	
		γ	γ'	γ	γ'	Elongated γ'	γ	γ'
Mo	0.3	0.5	0.3	0.7	0.4	0.3 ± 0.1	0.3	0.0
Hf	0.0 **	0.2	0.1	0.0	0.1	0.1	0.0	0.0
Ta	3.0	1.5	4.5	2.0	4.6	5.0 ± 1.1	3.6	4.6
W	1.9	4.0	2.7	2.2	2.6	2.5 ± 0.3	3.4	2.4
Re	2.4	6.0	1.1	7.6	1.1	1.0 ± 0.1	5.9	0.0
Ni	Bal.	Bal.	Bal.	Bal.	Bal.	Bal.	Bal.	Bal.

The exact amounts of Nb * and Hf ** are 0.04 and 0.001 at. pct, respectively.

For investigation of the as-cast microstructures of the blades, the components were removed from the gating system prior to heat treatment and cut out by wire-guided electro-discharge machining (EDM). Then, they were mounted, mirror-polished, etched, and ultrasonically cleaned in ethanol for 5 min for microstructural investigation.

Firstly, the as-cast tip of a blade was observed without any polishing or etching process, and the etched samples were then observed using a high-resolution scanning electron microscope (field emission (FE)-SEM, FEI Quanta 3D dual beam FIB-SEM, ThermoFisher Scientific, Hillsboro, OR, USA) equipped with an energy dispersive X-ray spectroscopy (EDX) system and a focused ion beam (FIB) facility. After SEM observation, TEM samples were fabricated in the same chamber by an in situ FIB lift-out technique [23,24]. As the superalloy has more than 10 alloying elements and some have close proximity characteristic X-rays (M_α, keV), such as Hf (1.644), Ta (1.709), W (1.774), and Re (1.842) [6,25], a high-resolution transmission electron microscope (FE-TEM, FEI Tecnai F20, ThermoFisher Scientific, Hillsboro, OR, USA) equipped with a scanning mode (STEM) and an EDX system was used at an operational voltage of 200 kV. Chemical compositions of the regions of interest were acquired by silicon drift detectors installed into the STEM with a nominal probe size of about 2 nm from more than 10 analysis areas to provide sufficient statistical confidence. These data were quantified using the analysis software (Oxford AZtecTEM, Oxford Instruments, High Wycombe, UK) installed on the equipment, which can perform a standardless analysis [26] and resolve differences of more than 0.03 keV by the deconvolution of overlapping elements and background removal [19,27]. To avoid or minimize microstructural changes in the irradiated area, TEM samples were cooled with liquid nitrogen during observation [24].

3. Results and Discussion

Figure 1 shows a typical microstructure of an as-cast nickel-based single crystal turbine blade. Through the whole turbine blade, dendrites were well developed along the specific {001} direction during casting and they were clearly visible at the tip of a blade, as shown in Figure 1a. The figure also shows a typical microstructure with mainly one dendrite after epoxy resin mounting, polishing, and etching. The dendrite with bright contrast and the interdendritic region with relatively dark contrast were clearly distinguishable at this magnification. The general dendritic microstructure and its formation mechanism are well understood and have been described elsewhere [1,3,4,12,28]. Figure 1c,d clearly show the microstructures at the dendrite core and in the interdendritic region. It should be emphasised that the micrographs were acquired exactly at the same magnification. The dendrite core shows almost uniform bright contrast at a low magnification of 5000× (the insert in Figure 1c). However, an image acquired at a higher magnification of 25,000× reveals a number of particles (γ' phase) of dark contrast and this γ' phase was not uniformly precipitated in the core because the turbine blade was only cast without further processes such as solution and aging heat treatments, which form the more familiar microstructure composed of uniformly precipitated γ' and thin γ channels. It should be noted that similar micrographs were acquired through the whole core region, which means that the γ' phase in the core was not well developed during casting. Compared with the core, the interden-

dritic region showed a quite different microstructure even at a low magnification of 5000× (the insert in Figure 1d); there are a number of coarse or elongated γ' particles (see also Figure 2). The main image in Figure 1d, which was acquired at the same magnification as Figure 1c, shows a clearly different morphology of bright γ channels and dark γ' particles. These observation results suggest that the morphology of the core and the interdendritic regions is quite different and, consequently, the formation mechanism of the core and the interdendritic region is also probably different.

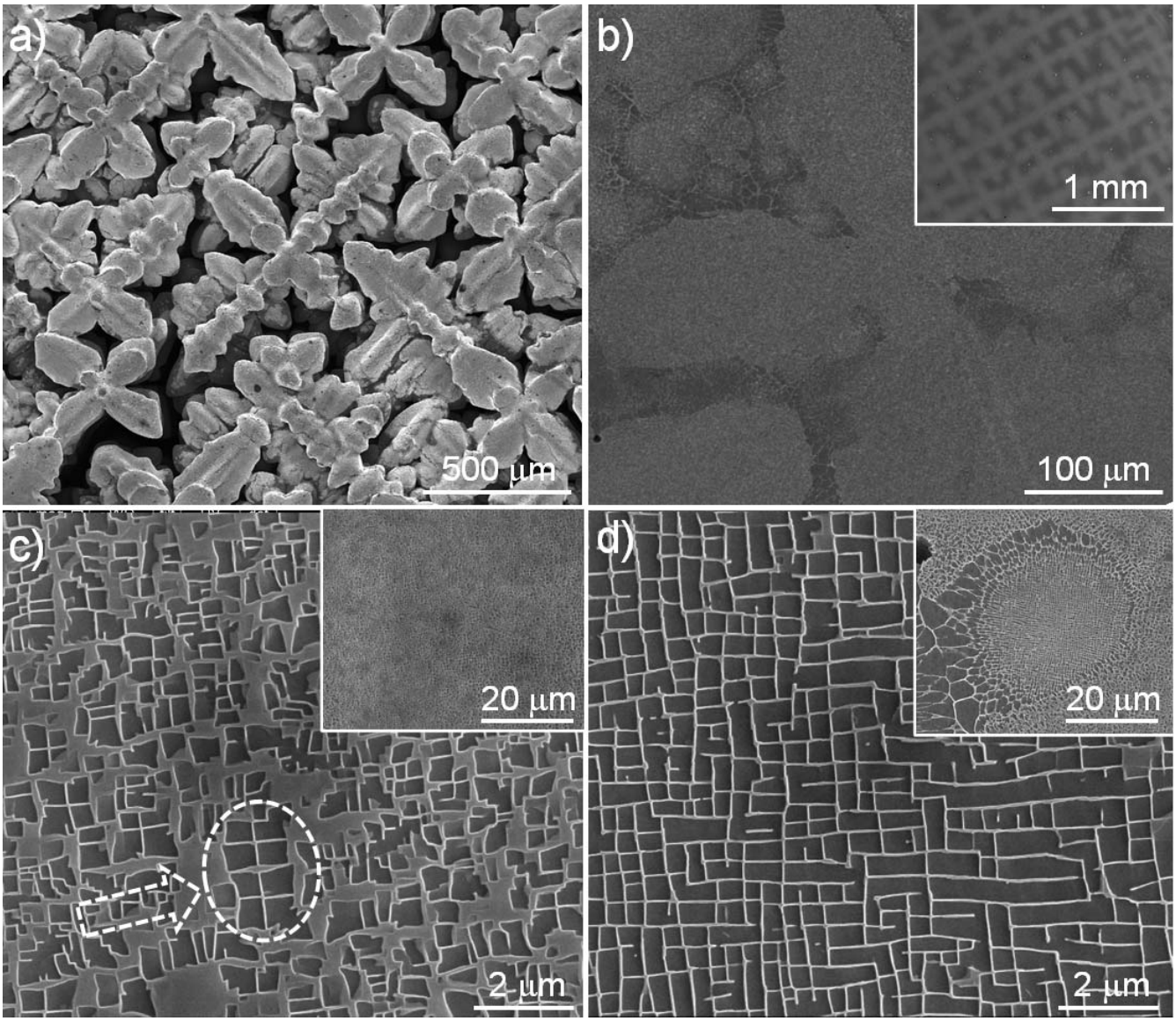

Figure 1. General images of a dendritic microstructure formed in a nickel-based single crystal superalloy: (**a**) as-cast dendrites found at the tip of a turbine blade at a low magnification image; (**b**) a dendrite after epoxy mounting, polishing, and etching with an insert showing a general morphology of dendrites; (**c**) a magnified image acquired at the dendrite core with an insert of a low magnification image; (**d**) a magnified image of an interdendritic region with a low magnification image. Note that in panels (**c**,**d**), the general and the magnified images were acquired at the same magnification.

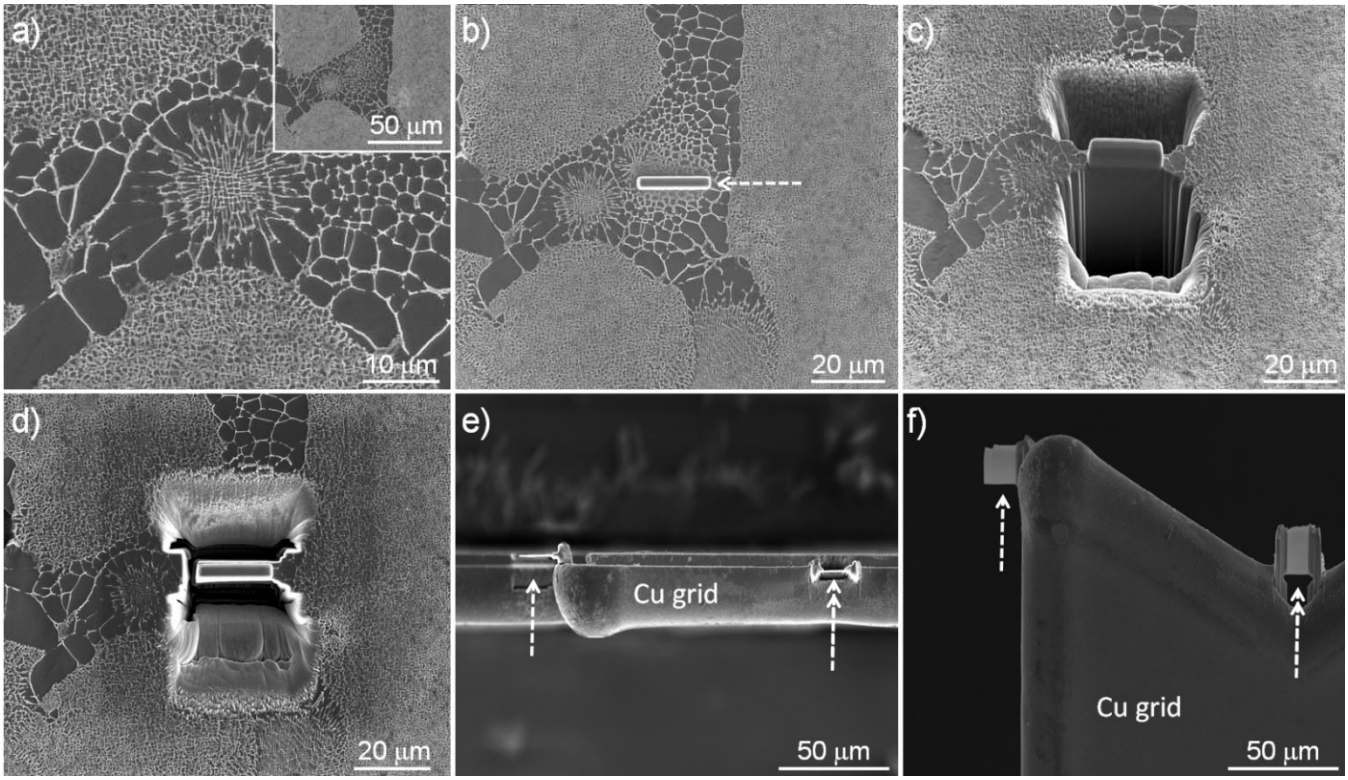

Figure 2. A series of a FIB lift-out technique for TEM sample preparation: (**a**) a plain view of an interdendritic region to be processed with an insert acquired at a low magnification; (**b**) a plain view showing platinum deposition on a small area of 20 × 4.5 μm^2 marked with an arrow; (**c**,**d**) a typical milling process with a tilting view of gradual trenches near the platinum-deposited area; (**c**) a plain view of the area prior to cutting the remaining right side; the lamella was then lifted out and placed on a copper grid by a typical FIB lifting-out process; (**e**) two different lamellae on the same copper grid; and (**f**) a tilting view of the two lamellae prior to final thinning and cleaning. Note that in (**e**) and (**f**), two different lamellae were made from a dendrite core marked with a double arrow and an interdendritic region with an arrow, respectively. In panel (**f**), electron transparent areas show relatively brighter contrast.

It should be noted that the core region showed a relatively consistent microstructure through the whole turbine blade, while the interdendritic region showed different microstructure depending on the observation region; thus, another representative region was selected and observed, as shown in Figure 2. In this figure, the central region was the interdendritic region surrounded by three dendrites. Due to the different contrast, the interdendritic region is easily recognised. Compared to the core, there are a smaller number of relatively dark contrast particles. It should be emphasised that the size of these dark contrast particles near the interface of core/interdendritic region is larger than those in the centre of the interdendritic region. In addition, the centre of the interdendritic region shows a similar morphology of γ and γ' to the core in Figure 1d.

This formation of the large particles and regular morphology of γ and γ' has been considered to be probably due to either eutectic or peritectic reaction [10]. It was necessary to investigate the composition of γ and γ' in the interdendritic region to confirm the reaction. As previously stated, the inherit interaction volume (a few micrometres) during SEM-EDX analysis makes the measurement of the composition of γ and γ' difficult. Therefore, a specific TEM sampling method using a focused ion beam (FIB) lift-out technique was used. First of all, a region was selected (Figure 2a) and a platinum layer, which is marked with an arrow in Figure 2b, was deposited on the surface to protect the sample from ion beams during FIB milling and thinning. Then, a typical FIB lift-out technique was carried out

(Figure 2c,d), and, finally, the thin lamella was lifted out by a manipulator and placed on the left part of a copper grid (Figure 2e). Then, unlike the typical TEM preparation process, the lamella on the grid was not thinned further. Instead, in this study, another lamella was fabricated and placed on the same grid in the same chamber without removing the grid. This avoided any contamination of the first lamella during the second sample fabrication, made lamellae with almost the same thickness, and crucially allowed observation of the lamellae under the same observation and analysis conditions. To allow comparison of the compositions of the γ and γ' phases at the core and the interdendritic region, the second lamella was fabricated from the core and placed on the central part of the grid, which is marked with a double arrow in Figure 2e. Following this, the lamellae were thinned to almost the same thickness. Figure 2f shows two lamellae on a copper grid. The bright region in each lamella is electron-transparent during TEM observation. After additional milling and cleaning, the TEM sample preparation was completed and, finally, plain view SEM images from the lamellae were acquired to measure the thickness of two lamellae. Then, the sample was immediately observed by TEM to avoid any air contamination.

Figure 3 shows STEM-HAADF images acquired from two different regions of the core and the interdendritic region. The top bright layer in Figure 3a,c, indicates the protective platinum layer, which means that the region was preserved without any critical damage during FIB sampling. It should be noted that compared to a normal TEM sample, the lamellae were thinned less in order to preserve the whole cross section of the region of interest, even though this affected the image quality at high magnification. Nonetheless, it is clear that two different morphologies at the core (Figure 3a,b) and the interdendritic region (Figure 3c,d) are visible and distinguishable.

The core region shows an irregular morphology of the γ' phase in γ. The precipitation of γ' is affected by the elastic modulus anisotropy in the turbine blade and usually forms a cuboidal morphology [29]. However, in this study, the turbine blade was not fully heat-treated but as-cast. Therefore, there was not sufficient time to form the complete morphology composed of cuboidal γ' precipitation in the γ matrix due to the relatively short casting time compared to the aging heat treatment used for this alloy. By comparison, the interdendritic region showed a completely different microstructure. There are primarily three different regions, which were marked as 'A', 'B', and 'C': the first (A) was composed of several elongated γ' particles shown in the top and middle of Figure 3c, the second (B) was composed of relatively tiny and irregular γ' in the bottom of Figure 3c, and the third (C) contained γ' with relatively regular morphology on the right of Figure 3c,d. This observation was in good agreement with other SEM observation results of the interdendritic region, and the previous images in Figures 1 and 2.

Figure 4 shows several STEM-EDX spectra acquired from the TEM samples in Figure 3. As a comparison, the core region was also analysed. Figure 4a,b are spectra of γ' acquired from the core (Figure 4a) and the interdendritic region (Figure 4b), respectively. As expected, strong peaks of nickel, aluminium, and tantalum were detected.

However, it is hard to distinguish the spectrum of the core γ' from that of the interdendritic γ' region despite repeating the STEM-EDX analysis in over ten areas. Thus, STEM-EDX point analysis was performed on the γ in the core (Figure 4c) and in the interdendritic region (Figure 4d), respectively. Compared to the compositional results of γ', stronger peaks of chromium, cobalt, and rhenium were acquired.

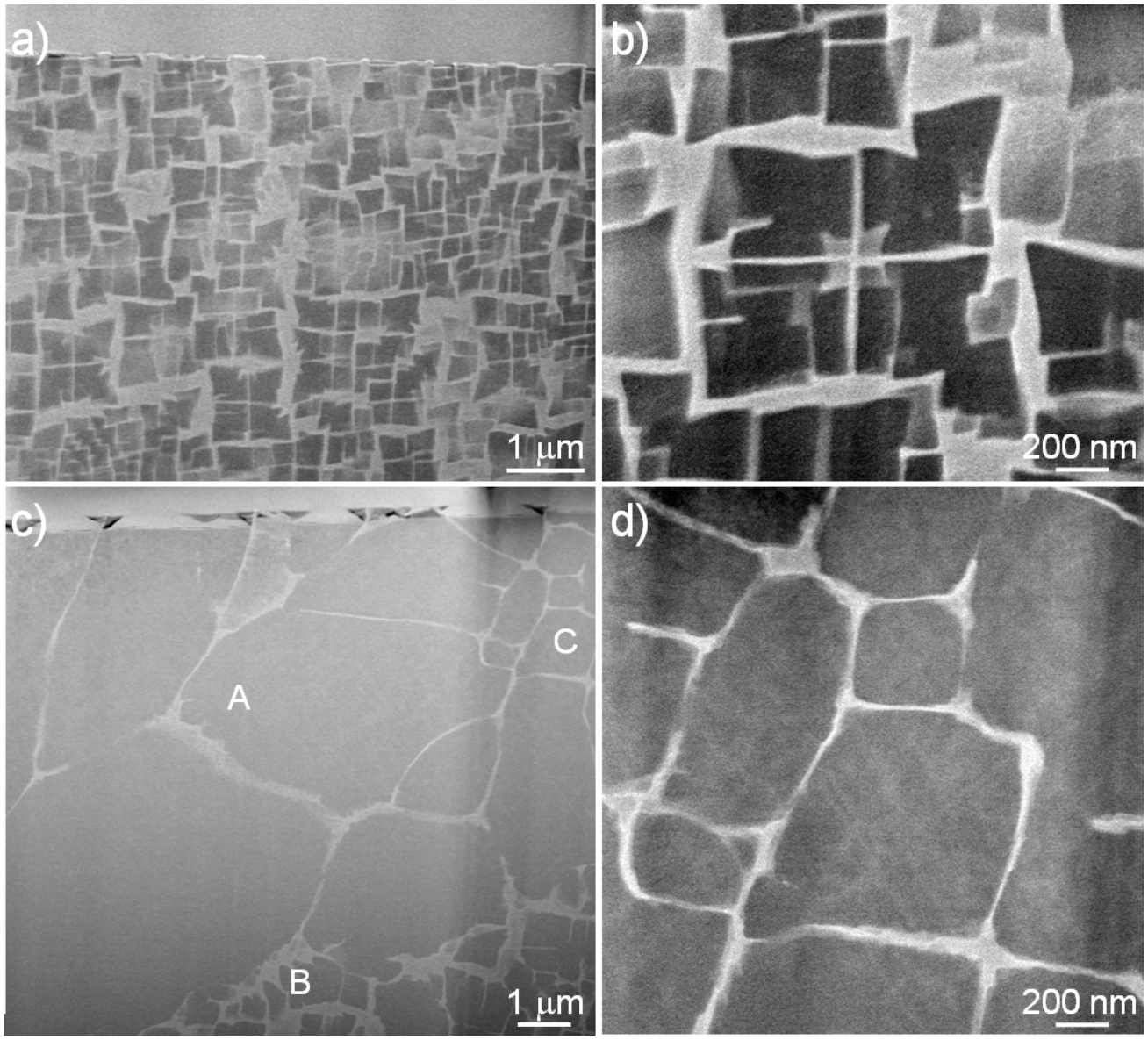

Figure 3. STEM-HAADF images acquired from the dendrite core (**a**,**b**) and the interdendritic region (**c**,**d**) of a turbine blade. Note that in the interdendritic region, there are three different regions, which are marked as 'A', 'B', and 'C'.

However, the spectra acquired from the γ also show a similar trend to that of the γ'; specifically, it is hard to distinguish the spectrum acquired from the γ in the core with that from the γ in the interdendritic region. Based on the spectra, the chemical compositions of γ and γ' in the core and in the interdendritic region were acquired and are summarised in Table 1. As shown in the spectra, the composition of γ' in the core is almost the same as that of γ' in the interdendritic region. In addition, the composition of γ in the core is also the same as that of γ in the interdendritic region. This result shows that when the γ' forms in the γ matrix, the composition of γ' is almost uniform regardless of the casting area, despite the bulk composition in these two regions being different due to the segregation during casting. It should be noted that even in the interdendritic region, some heavy alloying elements, such as rhenium and tungsten, were clearly detected, and they are also present in the γ' particles. For a comparison, the compositions acquired from fully heat-treated turbine blades are also included in Table 1.

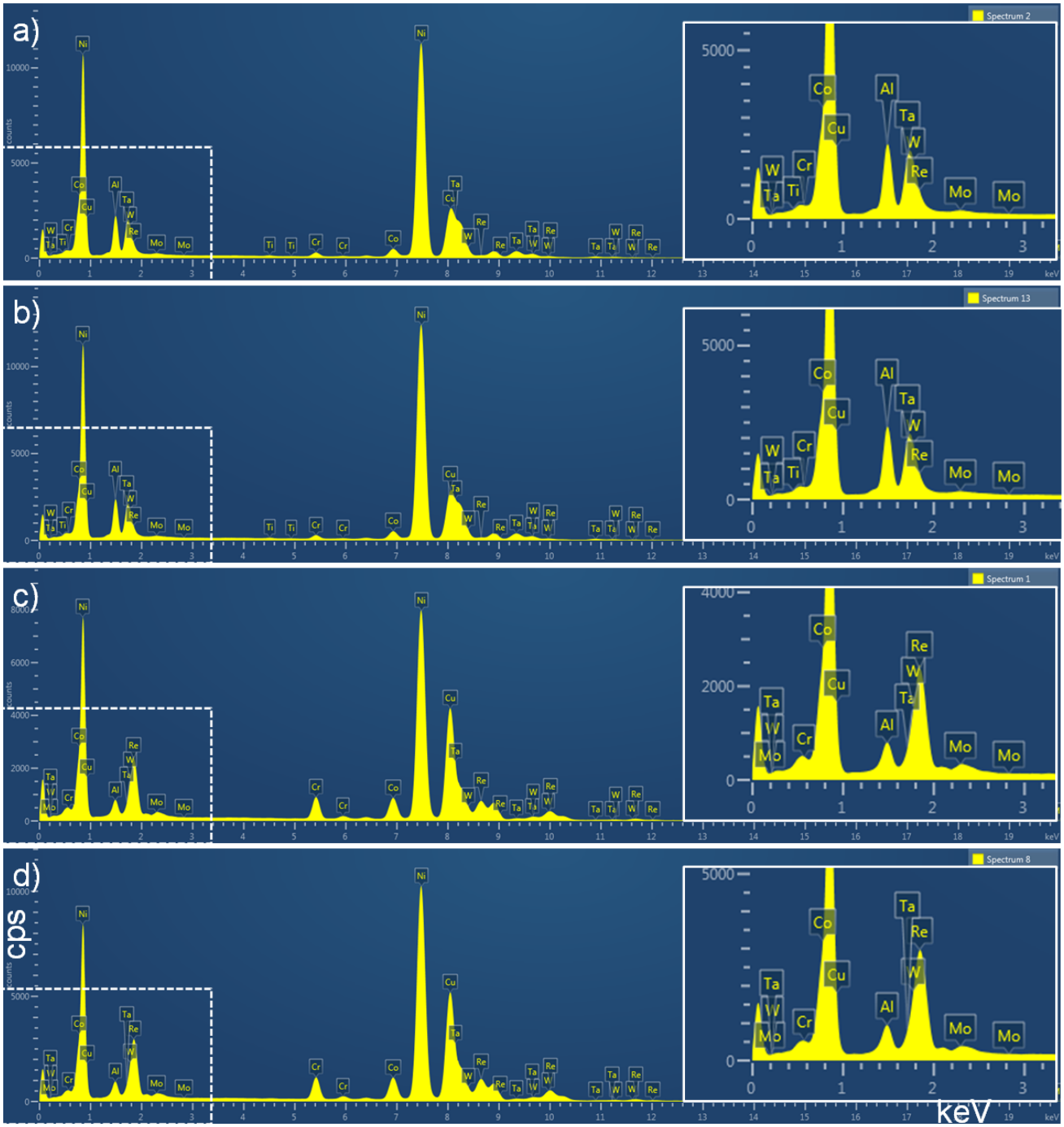

Figure 4. STEM-EDX spectra acquired at the dendrite core (**a**,**c**) and the interdendritic region (**b**,**d**): (**a**,**b**) gamma prime phase, and (**c**,**d**) gamma phase. The inserts are enlarged spectra from the marked range, respectively.

During STEM-EDX analysis, it should be noted that the spectrum and composition of γ' in the interdendritic region was acquired from the γ' on the right and the bottom regular type region in Figure 3c or in Figure 3d. STEM-EDX point analysis was also carried out on the elongated γ' in Figure 3c. The spectrum showed slightly high peaks of aluminium and titanium, but which are similar to the peaks in Figure 4. The composition acquired from the elongated γ' is also summarised in Table 1. It is clear that the amounts of aluminium and tantalum in the elongated γ' are slightly higher than those in the rest of the interdendritic region or in the core. It should be noted that the compositions of γ and γ' in the core

and the interdendritic region, where there is a mix of γ and γ′, remain the same with the general compositional differences being accommodated through the varying of the proportions of γ and γ′. However, the composition of the elongated γ′ in the interdendritic region was slightly different, with higher aluminium than the other γ′ areas. The general composition in these areas does not sit between the γ and γ′ compositions seen elsewhere, so the microstructure becomes made up of large areas of γ′ in an attempt to reach the preferred composition. The compositions of aluminium and tantalum were shown to be the most variable. These results demonstrate that the last portion to solidify in the casting has to accommodate all the γ′ forming elements at the expense of forming no further γ; hence, the size of the γ′ particles.

Based on the chemical compositions in Table 1, the partitioning behaviour of main alloying elements is summarised in Figure 5. As is well known, aluminium is strongly partitioned to the γ′, Figure 5a, but is of consistent composition, except for the interdendritic elongated γ′ where there is a higher concentration. Chromium (Figure 5b) and cobalt (Figure 5c) show different behaviour to aluminium and it is difficult to identify a trend between the dendrites, the interdendritic regions, and the fully heat-treated material. Rhenium (Figure 5d) shows relatively high concentrations in the interdendritic γ when compared to γ in other locations and the heat-treated state, but as there is relatively little γ to accommodate the rhenium present, the composition here is increased. The presence of excess rhenium here means that it is not necessary for rhenium, which has the slowest diffusion rate of the alloying elements in the base material [30–32], to diffuse long distances from the core to the interdendritic region to enable a uniform microstructure composed of thin γ channels and a fine precipitate of γ′ during subsequent heat treatment.

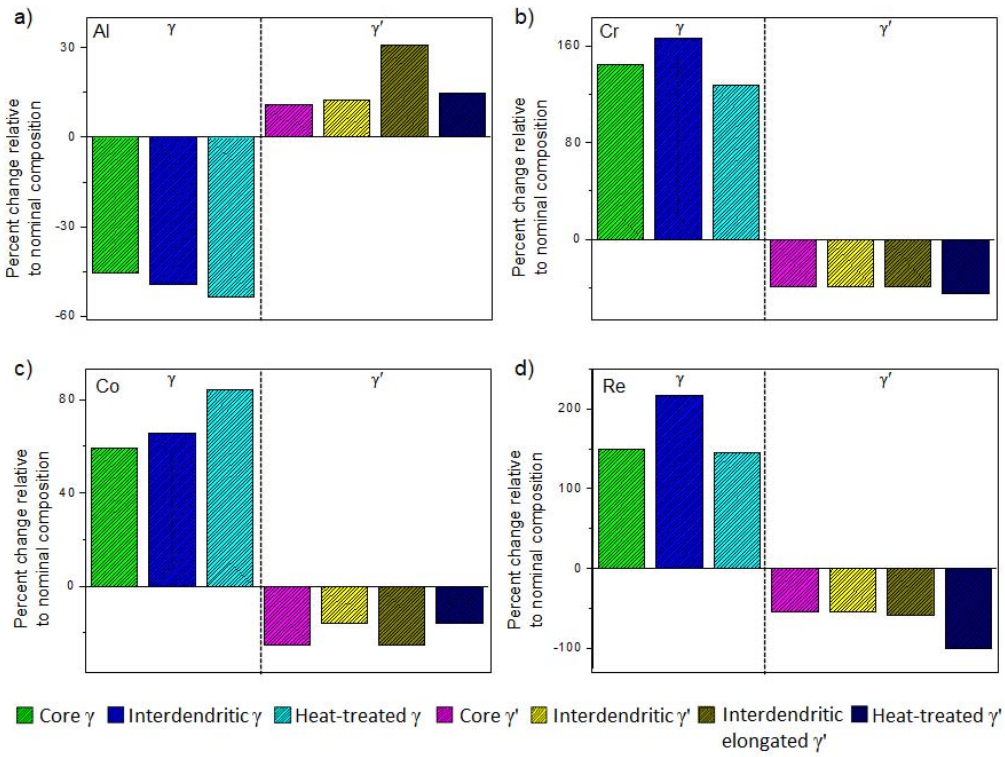

Figure 5. Percent changes relative to nominal composition of (**a**) Al, (**b**) Cr, (**c**) Co, and (**d**) Re based on Table 1.

It is well documented that during solidification through dendritic growth, the higher melting point elements preferentially solidify in the dendrites, whereas the lower melting point elements are preferentially pushed into the interdendritic areas. This is true in nickel-based superalloys but this does not lead to total partitioning, only changes in local composition in line with these drivers [4]. The alloy can be seen to behave as a

pseudo-binary with two preferred compositions; the local composition only changes the proportions of γ and γ' seen locally rather than changing the compositions of the γ and γ' to accommodate the local composition. This description explains the formation of the observed microstructures in both the core and interdendritic areas. It also explains the large areas of γ' that form adjacent to the dendrites, because this is the area of the casting that is richest in aluminium as it is ejected from the solidifying dendrite cores; the amount of aluminium present is higher than the preferred amount of aluminium in equilibrium γ' and hence γ' is formed. The rhenium in the interdendritic regions is ejected into the small amount of γ available, hence increasing the rhenium content in the γ in these regions.

4. Conclusions

A number of conclusions can be drawn from this work:

1. The core region showed a relatively uniform microstructure, whereas the interdendritic region showed a range of microstructures depending on the area observed.
2. There is a preferred composition of γ and γ' in the alloy and these compositions are seen in both the as-cast and the fully solution heat-treated material. These preferred compositions are not substantially influenced by the local composition.
3. During the formation of the γ' precipitate, the amount of γ' formed is based on the balance of these preferred compositions within the local composition
4. Only where the local composition cannot accommodate a balance of γ and γ' does the microstructure comprise large areas of γ' and deviate away from the preferred compositions.

Author Contributions: Conceptualization, K.P. and P.W.; methodology, K.P.; investigation, K.P.; resources, P.W.; writing—original draft preparation, K.P.; writing—review and editing, P.W. All authors have read and agreed to the published version of the manuscript.

Funding: This work was supported by the Engineering and Physical Sciences Research Council [grant number EP/T018518/1].

Institutional Review Board Statement: Not applicable.

Informed Consent Statement: Not applicable.

Data Availability Statement: Not applicable.

Conflicts of Interest: The authors declare no conflict of interest.

References

1. Durand-Charre, M. *The Microstructure of Superalloys*; OPA: Amsterdam, The Netherlands, 1997.
2. Bar-Cohen, Y. *High Temperature Materials and Mechanisms*; CRC Press: New York, NY, USA, 2014.
3. Geddes, B.; Leon, H.; Huang, X. *Superalloys: Alloying and Performance*; ASM International: Materials Park, OH, USA, 2010.
4. Reed, R.C. *The Superalloys: Fundamentals and Applications*; Cambridge University Press: Cambridge, UK, 2006.
5. Smith, W.F. *Structure and Properties of Engineering Alloys*, 2nd ed.; McGraw-Hill Book Co.: New York, NY, USA, 1994.
6. Warren, P.; Cerezo, A.; Smith, G. An atom probe study of the distribution of rhenium in a nickel-based superalloy. *Mater. Sci. Eng. A* **1998**, *250*, 88–92. [CrossRef]
7. Giamei, A.F.; Anton, D. Rhenium additions to a Ni-base superalloy: Effects on microstructure. *Met. Mater. Trans. A* **1985**, *16*, 1997–2005. [CrossRef]
8. Yeh, A.; Tin, S. Effects of Ru and Re additions on the high temperature flow stresses of Ni-base single crystal superalloys. *Scr. Mater.* **2005**, *52*, 519–524. [CrossRef]
9. Reed, R.; Tao, T.; Warnken, N. Alloys-By-Design: Application to nickel-based single crystal superalloys. *Acta Mater.* **2009**, *57*, 5898–5913. [CrossRef]
10. D'Souza, N.; Dong, H. Solidification path in third-generation Ni-based superalloys, with an emphasis on last stage solidification. *Scr. Mater.* **2007**, *56*, 41–44. [CrossRef]
11. Kearsey, R.M.; Beddoes, J.C.; Jones, P.; Au, P. Compositional design considerations for microsegregation in single crystal superalloy systems. *Intermetallics* **2004**, *12*, 903–910. [CrossRef]
12. Feng, Q.; Nandy, T.; Tin, S.; Pollock, T. Solidification of high-refractory ruthenium-containing superalloys. *Acta Mater.* **2003**, *51*, 269–284. [CrossRef]
13. Cameca. Introduction to EPMA. Available online: https://www.cameca.com/products/epma/technique (accessed on 6 March 2015).

14. Laigo, J.; Christien, F.; Le Gall, R.; Tancret, F.; Furtado, J. SEM, EDS, EPMA-WDS and EBSD characterization of carbides in HP type heat resistant alloys. *Mater. Charact.* **2008**, *59*, 1580–1586. [CrossRef]
15. Shimizu, R.; Ze-Jun, D. Monte Carlo modelling of electron-solid interactions. *Rep. Prog. Phys.* **1992**, *55*, 487–531. [CrossRef]
16. Demers, H.; Poirier-Demers, N.; Couture, A.R.; Joly, D.; Guilmain, M.; de Jonge, N.; Drouin, D. Three-dimensional electron microscopy simulation with the CASINO Monte Carlo software. *Scanning* **2011**, *33*, 135–146. [CrossRef]
17. Matuszewski, K.; Rettig, R.; Matysiak, H.; Peng, Z.; Povstugar, I.; Choi, P.; Müller, J.; Raabe, D.; Spiecker, E.; Kurzydłowski, K.; et al. Effect of ruthenium on the precipitation of topologically close packed phases in Ni-based superalloys of 3rd and 4th generation. *Acta Mater.* **2015**, *95*, 274–283. [CrossRef]
18. Kim, K.H. FIB serial milling and lifting out of fine inclusions in an intensively melt sheared aluminum alloy. *Mater. Lett.* **2014**, *117*, 74–77. [CrossRef]
19. Kim, K.; Withey, P.; Griffiths, W.D. Detection of an Intermediate layer containing a rhenium-rich particle at grain boundaries formed within single crystal nickel-based superalloys. *Met. Mater. Trans. A* **2015**, *46*, 1024–1029. [CrossRef]
20. Kim, K.; Withey, P.A. Microstructural Investigation of the formation and development of topologically close-packed phases in a 3rd generation nickel-base single crystal superalloy. *Adv. Eng. Mater.* **2017**, *19*, 1700041. [CrossRef]
21. Wu, X.; Makineni, S.K.; Liebscher, C.H.; Dehm, G.; Mianroodi, J.R.; Shanthraj, P.; Svendsen, B.; Bürger, D.; Eggeler, G.; Raabe, D.; et al. Unveiling the Re effect in Ni-based single crystal superalloys. *Nat. Commun.* **2020**, *11*, 389. [CrossRef] [PubMed]
22. Lapington, M.T.; Crudden, D.J.; Reed, R.C.; Moody, M.P.; Bagot, P.A.J. Characterization of phase chemistry and partitioning in a family of high-strength nickel-based superalloys. *Met. Mater. Trans. A* **2018**, *49*, 2302–2310. [CrossRef]
23. Kim, K.; Watanabe, M.; Kawakita, J.; Kuroda, S. Grain refinement in a single titanium powder particle impacted at high velocity. *Scr. Mater.* **2008**, *59*, 768–771. [CrossRef]
24. Kim, K. Formation of fine clusters in high-temperature oxidation of molten aluminum. *Met. Mater. Trans. A* **2014**, *45*, 3650–3660. [CrossRef]
25. JEOL. Energy Table for EDS Analysis. 2013. Available online: https://www.unamur.be/services/microscopie/sme-documents/Energy-20table-20for-20EDS-20analysis-1.pdf (accessed on 6 February 2022).
26. Kim, K.; Withey, P. Formation of an Intermediate layer between grains in nickel-based superalloy turbine blades. *Met. Mater. Trans. A* **2017**, *48*, 2932–2942. [CrossRef]
27. Oxford Instruments. AZtecEnergy: The Ultimate EDS System. 2013. Available online: http://www.oxford-instruments.com/products/microanalysis (accessed on 28 September 2013).
28. Dantzig, J.A.; Rappaz, M. *Solidification*; CRC Press: Boca Raton, FL, USA, 2009.
29. Ricks, R.A.; Porter, A.J.; Ecob, R.C. The growth of γ' precipitates in nickel-base superalloys. *Acta Metall.* **1983**, *31*, 43–53. [CrossRef]
30. Janotti, A.; Krčmar, M.; Fu, C.L.; Reed, R.C. Solute diffusion in metals: Larger atoms can move faster. *Phys. Rev. Lett.* **2004**, *92*, 085901. [CrossRef] [PubMed]
31. Park, K.; Withey, P. Observation of the dissolution of topologically close packed phases by an additional heat treatment in third generation nickel-based single crystal superalloy turbine blades. *Adv. Eng. Mater.* **2018**, *20*, 1700987. [CrossRef]
32. Erickson, G.L. The development and application of CMSX (R)-10. In *Superalloys*; The Minerals, Metals & Materials Society: Pittsburg, PA, USA, 1996.